# Nanoscale

Accepted Manuscript


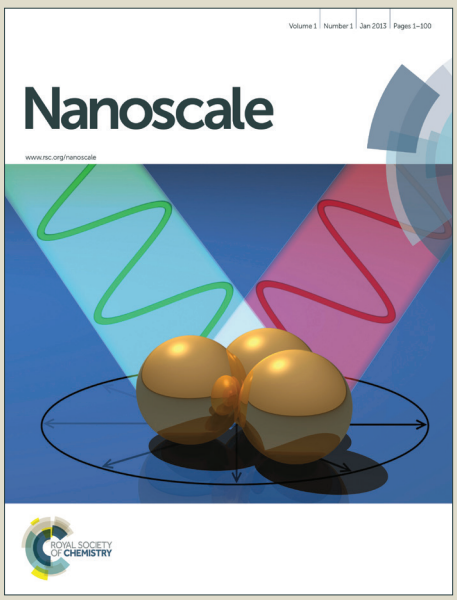





ROYAL SOCIETY OF CHEMISTRY

www.rsc.org/nanoscale

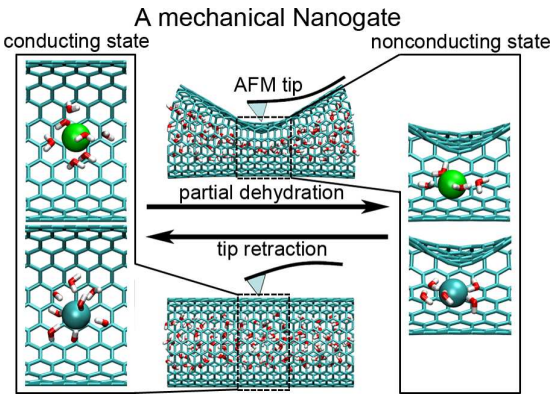


Ion conduction in nanofluidic devices can be reversibly controlled by regulating ion hydration state with an AFM-tip deformable nanogate.

Cite this: DOI: 10.1039/c0xx00000x

www.rsc.org/xxxxxx

ARTICLE TYPE

# A mechanical nanogate based on a carbon nanotube for reversible control of ion conduction

**Zhongjin He,[a] Ben Corry,[b] Xiaohua Lu[c] and Jian Zhou*[a]**

***Received (in XXX, XXX) Xth XXXXXXXXX 20XX, Accepted Xth XXXXXXXXX 20XX***

**DOI: 10.1039/b000000x**

Control of mass transport through nanochannels is of critical importance in many nanoscale devices and nanofiltration membranes. The gates in biological channels, which control the transport of substances across cell membranes, can provide inspirations for this purpose. Gates in many biological channels are formed by a constriction ringed with hydrophobic residues which can prevent ion conduction even when they are not completely physically occluded. In this work, we use molecular dynamics simulations to design a nanogate inspired by this hydrophobic gating mechanism. Deforming a carbon nanotube (12,12) with an external force can form a hydrophobic constriction in the tube centre that controls ion conduction. The simulation results show that increasing the magnitude of the applied force narrows the constriction and lowers the fluxes of $K^+$ and $Cl^-$ found under an electric field. With the exerted force lager than 5 nN, the constriction blocks the conduction of $K^+$ and $Cl^-$ due to partial dehydration while allowing for a noticeable water flux. Ion conduction can revert back to the unperturbed level upon the force retraction, suggesting the reversibility of the nanogate. The force can be exerted by available experimental facilities, such as atomic force microscope (AFM) tips. It is found that partial dehydration in a continuous water-filled hydrophobic constriction is enough to close the channel, while full dewetting is not necessarily required. This mechanical deformed nanogate has many potential applications, such as a valve in nanofluidic systems to reversibly control ion conduction and a high-performance nanomachine for desalination and water treatment.

## Introduction

The controlled transport of water and ions through biological channels plays a critical role in biology, such as in osmoregulation and the electrical activities of cells.[1] It is desirable in modern nanotechnology, especially in nanofluidic systems, to have nanochannels through which transport can be tightly controlled. Ideally, we would like to have nanochannels that can be opened and closed to facilitate or prevent transport, and therefore, a nanovalve or nanogate needs to be designed to achieve this purpose. However, the transport in the channels of nanometer dimension is quite different from that in macroscopic channels, which makes the design of nanovalve or nanogate a challenge. Experimental and theoretical studies[2-4] have shown that the gas and liquid flow through carbon nanotubes (CNTs) is several orders of magnitude faster than would be predicted from conventional fluid-flow theory. Previous simulation studies[5,6] have indicated that water transport in single-file form in CNT(6,6) can effectively resist the disturbances of tube deformation or external charge and be interrupted only by strong perturbations. It is found that the water permeation across nanochannel can be affected greatly by the external structure, which is quite different from the macroscopic scenario.[7] In addition, liquid-vapor oscillations of water have been observed in hydrophobic nanochannels.[8] Previous investigations[9,10] focused primarily on the electroosmotic flow through charged nanochannels found that the properties of the nanochannel wall affect the flow profoundly. Recently, the ion permeation dynamics and the effects of several factors on the ion transport properties in CNTs have been studied systematically with molecular dynamics (MD) simulations.[11-14] Experimentally, the ion transport properties across silicon nitride nanochannels[15] and CNTs[16] under an external electric field were evaluated, and the results showed that the mobilities of ions within these nanochannels were much higher than the bulk mobility.

Nanovalves have a wide range of potential applications. Microfluidic systems known as "lab-on-a-chip" have been developed as tools for accurate chemical analysis,[17] and require femtoliter liquid be processed, which can realized by nanovalve devices. Simulation studies[18-20] showed that the separation of gases and ions, and signal processing can be achieved by CNT-based nanogates. Great efforts have been made to fabricate mechanised silica nanoparticels as nanovalves,[21] which can serve as a smart drug delivery system. In addition, nanovalves made of polymer-grafted nanopores[22] or channel proteins[23,24] are able to control flows in nanochannels. Compared with the nanovalves mentioned above, CNT-based nanovalve have some advantages, such as fast mass transport ability at the open state,[2,3] unique hydrophobicity, 1D hollow and regular structure, controllable

diameter and length,[25] and easy chemical functionalization.[26] Thus, several efforts have recently been made to manipulate the mass transport in CNTs. Majumder et al.[27] fabricated membranes composed of CNTs functionalized with charged molecular tethers, which exhibited voltage gated control of ionic transport. Yu et al.[28] found that gated ion transport through dense CNT membranes can be achieved by regulating the water wettability of CNT hydrophobic surfaces by ultrasound or temperature change. The simulation work of Gong et al.[29] demonstrated that it was possible to control ion-selective transport through a nanotube by an external charge. Based on the knowledge on transport in nanochannels accumulated by previous efforts, this study aims to design a nanogate to control ion conduction in nanochannels.

Biological ion channels are able to provide inspirations for designing nanogates. Almost all the biological channels are gated, *i.e.*, they contain a region that can switch between open and closed states and thus control the transport of ions, water and other species in or out of cells.[1] This open-closed transition is implemented by conformational changes in response to external signals, including changes in transmembrane potential, ligand binding or mechanical stress. The crystal structures of several ion channels showed that their gates are formed by a constricting girdle lined by hydrophobic residues.[30-33] Surprisingly, these gates are not completely physically occluded even in the functionally closed state, which is quite different from the effect of steric occlusion in macroscopic channel gating. Subsequent simulation studies[34-40] found that the narrow hydrophobic girdle is almost fully 'dewetted' in the closed state, and that an ion passing through this region has to shed water molecules from its hydration shell without any compensating interactions with polar groups on the pore walls. This results in an insurmountable energy barrier for ion transport. This hydrophobic gating mechanism is found to operate in a number of ion channels, including nicotinic acetylcholine receptor channel nAChR,[34,35] KcsA potassium channel,[36] ligand-gated ion channel ELIC[38] and bacterial mechanosensitive channel MscS and MscL.[41,42] Theoretical studies[43,44] showed that a hydrophobic model pore with diameter lower than a critical value can effectively block the passage of water and ions. Ion hydration states play a dominant role in determining ion transport in biological channels and synthetic nanochannels, which is demonstrated by theoretical simulations and experiments.[45-55] Additionally, the different dehydration energies of ions endow narrow hydrophobic nanopores with an intrinsic ion selectivity.[14,56,57] However, it is difficult to regulate ionic hydration states in nanochannels to control ion conduction.

Inspired by the hydrophobic gating mechanism in biological channels, here, we use MD simulations to design a nanogate to control the conduction of $K^+$ and $Cl^-$ based on the hydrophobic pore of CNT(12,12). The tube was deformed by an external force, which can be exerted by an atomic force microscope (AFM) tip. A hydrophobic constriction formed in the tube centre can serve as a nanogate to block ion conduction while allowing water transport. This nanogate is reversible, as the constriction can recover upon the force retraction. When the transport of ions is blocked, the nanogate can still allow for a water flux of about 6 molecules per ns, which may be suitable for seawater desalination. This novel nanogate could act as a functional component in ionic nanofluidic systems and water-processing devices.

## Simulation details

A (12,12) CNT was embedded along the z axis between two graphite sheets to form a simplified ion channel, as shown in Fig. 1. The effective radius of CNT(12,12) is 0.64 nm, close to the radii of the hydrophobic regions of nAChR and $K^+$ channel MthK in their open states.[58,59] The length of the nanotube was chosen to be 3.45 nm, comparable to the thickness of cell membranes. The channel was located between z = -1.72 nm and z = 1.72 nm with the centre at z = 0, and connected two reservoirs containing 1 M KCl solution. A force was applied to the middlemost carbon atom in the top side of the nanotube. The carbon atoms at the bottom of the nanotube were fixed. As a result, this atom and its neighboring carbon atoms were pushed away from their initial equilibrium positions. A constriction with effective radius $R_{min}$ (excluding a carbon atom van der Waals radius of 0.17 nm) was formed in the midway of the CNT(12,12) after energy relaxation for each external force. Using different strengths of the applied force, deformed tubes were constructed with $R_{min}$ = 0.19, 0.21, 0.23, 0.28, 0.33, 0.42 and 0.52 nm.

In the simulations, carbon atoms in the CNT(12,12) and graphite sheets were modeled as $sp^2$-like aromatic carbons in the CHARMM27 force field,[60] following the previous simulations.[45,51] The TIP3P water model[61] was employed. The parameters for $K^+$ and $Cl^-$ were also taken from the CHARMM27 force field. Although nonpolarizable models for water and ions cannot describe the structuring of halide ions ($Cl^-$ in this work) at the solution-CNT interface[62] as well as polarizable models do,[63] Beu's simulation work[64] has demonstrated that consideration of polarizability have little relevance to the dynamic properties of ions in CNTs, such as ionic fluxes, and that using nonpolarizable models can obtain appreciable accuracy. In addition, computational expense of using polarizable models is several times of non-polarizable ones. Therefore, nonpolarizable models were adopted in this work to explore the transport of ions through CNT(12,12). Periodic boundary conditions were imposed in all the directions. The short-range van der Waals interaction was cut off at 1.0 nm. The long-range electrostatic interactions were computed with particle mesh Ewald method.[65] Trajectories were integrated using the leapfrog scheme with a time step of 2 fs.

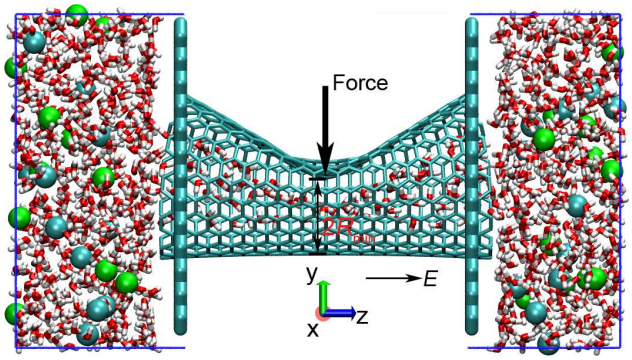


**Fig. 1** The simulation model. CNT(12,12) and the graphite sheets are in cyan. Water molecules are depicted as red and white rods. The green and cyan balls represent $K^+$ and $Cl^-$, respectively. An external force is applied on an atom of CNT(12,12) and a constriction with effective radius $R_{min}$ is

formed at the tube centre. A uniform electric field $E$ in the positive direction of z-axis is adopted.

After energy minimization, the system was equilibrated for 5 ns under NPT ensemble to obtain proper water density in CNT(12,12), during which harmonic constraints with spring constant 1000 kJ/mol/nm$^2$ were applied to the carbon atoms. The temperature of the system is maintained at 300 K by using the Nosé-Hoover thermostat[66] with a time constant of 0.1 ps. The Parrinello-Rahman scheme[67] with a time constant of 5.0 ps was employed to regulate the pressure of the system at 1 bar. The size of the system was 3.57×3.50×6.32 nm$^3$ after NPT equilibration. NVT ensemble was implemented in the subsequent simulations. Coordinates were stored every 1 ps for analysis. All the simulations were performed with GROMACS4.5.4 software.[68]

To evaluate the gating property of the CNT(12,12) with different degree of deformation, a uniform electric field, $E$, applied along the tube in the positive direction of z-axis was used to drive the ionic fluxes. The deformed CNT(12,12) was held stationary to keep its diameter steady. To simulate the process of force retraction from the tube, position constraints were removed from all the carbon atoms except those at the tube bottom. A strong electric field ($E$ = 0.1, 0.15 and 0.2 V/nm) was used in the 105 ns MD simulation so that enough ion passage events could be observed. The data from the last 100 ns were collected for analysis. The potential of mean force (PMF) of each ion passing through CNT(12,12) with deformation under equilibrium conditions ($E$ = 0) was determined using umbrella sampling.[69] The ion was moved through positions from z = -2.5 nm to z = 2.5 nm in 0.05 nm increments and held in position using a harmonic potential of 4000 kJ/mol/nm$^2$. For each window, a 1 ns simulation was run and umbrella sampling data were collected at every integration step. The first 100 ps of each run was discarded as equilibration. The weighted histogram analysis method[70] (WHAM) was used to calculate PMF profiles with a tolerance of $10^{-6}$ and 200 bins along the z axis. All PMF profiles were one-ion profiles as no other ions entered the tube during the simulations.

To create the deformed nanotubes and to determine the magnitude of the external force required to achieve certain degree of deformation, steered molecular dynamics[71] (SMD) simulations were performed. Constant velocity SMD was first performed to deform CNT(12,12). Only the carbon atoms at the tube bottom were fixed as immobile reference for the SMD simulation. The middlemost carbon atom in the top side of CNT(12,12) was pushed toward the negative direction of the y-axis for about 2 ns, using a spring constant of 10000 kJ/mol/nm$^2$ and a pull rate of 0.001 nm/ps. Different spring constants and pulling velocities have been tried. The results showed that CNT(12,12) can only be deformed with relative large spring constant and the pulling velocity did not change the magnitude of the force needed to achieve certain degree of deformation but only the simulation time required to achieve certain deformation. Then the magnitude of the force was chosen from the force-deformation curve obtained in constant velocity SMD simulations, and was used in constant force SMD to confirm whether a certain deformation can be achieved under the action of such a force.

## Results and discussion

### Gating the ionic flux through the channel by deformation

Under the applied force on the tube, the CNT(12,12) was deformed laterally and a constriction was formed in the tube midway, as shown in Fig. 1. The inset of Fig. 2A shows the cross-sectional view of this constriction and its effective radius $R_{min}$. To determine the extent of tube deformation required to effectively close its pathway for ionic conduction, several configurations of CNT (12,12) with different deformation were considered, *i.e.*, $R_{min}$ = 0.52, 0.42, 0.33, 0.28, 0.23, 0.21 and 0.19 nm. The radius of CNT(12,12) without any deformation was 0.64 nm. The radius along the tube axis of CNT(12,12) with different deformation was computed using HOLE,[72] and pictured in Fig. 2A. The radius gradually decreases to $R_{min}$ when approaching the constriction in the tube centre (z = 0). The radii of the constricted channels is comparable to the biological counterparts of 0.3, 0.2, 0.12 and 0.35 nm, respectively, for the hydrophobic constrictions of nAChR,[30] KcsA,[58] ELIC[32] and MscS[33] in their closed states.

In response to the tube deformation, the number density distributions of water, $K^+$ and $Cl^-$ along the tube axis under the applied electric field $E$ = 0.1 V/nm are also changed, as shown in Fig. 2B, 2C and 2D. The shapes of the water number density curves are quite similar to those of the radius profiles shown in Fig. 2A, indicating that the density change originates from the radius change along the tube axis. The water number density is lowered when closing to the constriction position, and decreases with the narrowing radius of the constriction ($R_{min}$), depicted in Fig. 2B. The constrictions are always filled with watermolecules for all the considered values of $R_{min}$ and transitions between water-filled and empty states are not observed here as they have been in previous studies of narrow biological channels and synthetic hydrophobic nanopores.[34-40,44] This discrepancy may due to the relative larger pore size of the deformed CNT(12,12) compared with the pore sizes in these previous studies.

As shown in Fig. 2C and 2D, the number densities of $K^+$ and $Cl^-$ in the constriction (z = 0) descend with the decrease of $R_{min}$. For $R_{min}$ = 0.23, 0.21 and 0.19 nm, the ionic number density is almost 0, indicating that under $E$ = 0.1 V/nm the tube is closed to $K^+$ and $Cl^-$ when $R_{min}$ is less than 0.23 nm. In addition, for $R_{min}$ < 0.42 nm, the obvious asymmetry of ionic number density distribution about the constriction (z = 0) suggests that the tube provides a barrier to ion transport. As shown in Fig. 2C, $K^+$ moves in the positive direction of z axis (the same direction of $E$) and its passage through the tube is obstructed by the constriction; as a result, $K^+$ ions are enriched on the left side of constriction and a higher density is observed. Similarly, negatively charged $Cl^-$ moves in the negative direction of z axis (opposite to the direction of $E$) and the density is more pronounced on the right side of the constriction, shown in Fig. 2D.

To explore whether the ionic conduction through the channel of CNT(12,12) can be gated by deforming the tube, the flux of $K^+$ and $Cl^-$ through the tube with deformation under $E$ = 0.1 V/nm was analyzed, and the error bar of flux was calculated by dividing the simulation into equal 25 ns blocks. The results are displayed in Fig. 3. When the tube is slightly deformed ($R_{min}$ = 0.52 nm), the flux has little change. However, the flux drops sharply when $R_{min}$ decreases from 0.52 to 0.28 nm. For $R_{min}$ < 0.28 nm, the ionic flux is negligible. The tube is totally closed to $K^+$ and $Cl^-$ when $R_{min}$ = 0.19 nm. The flux of water is 6-8 molecules per ns when $R_{min}$ < 0.28 nm (Fig. S1A in the ESI†), implying that such

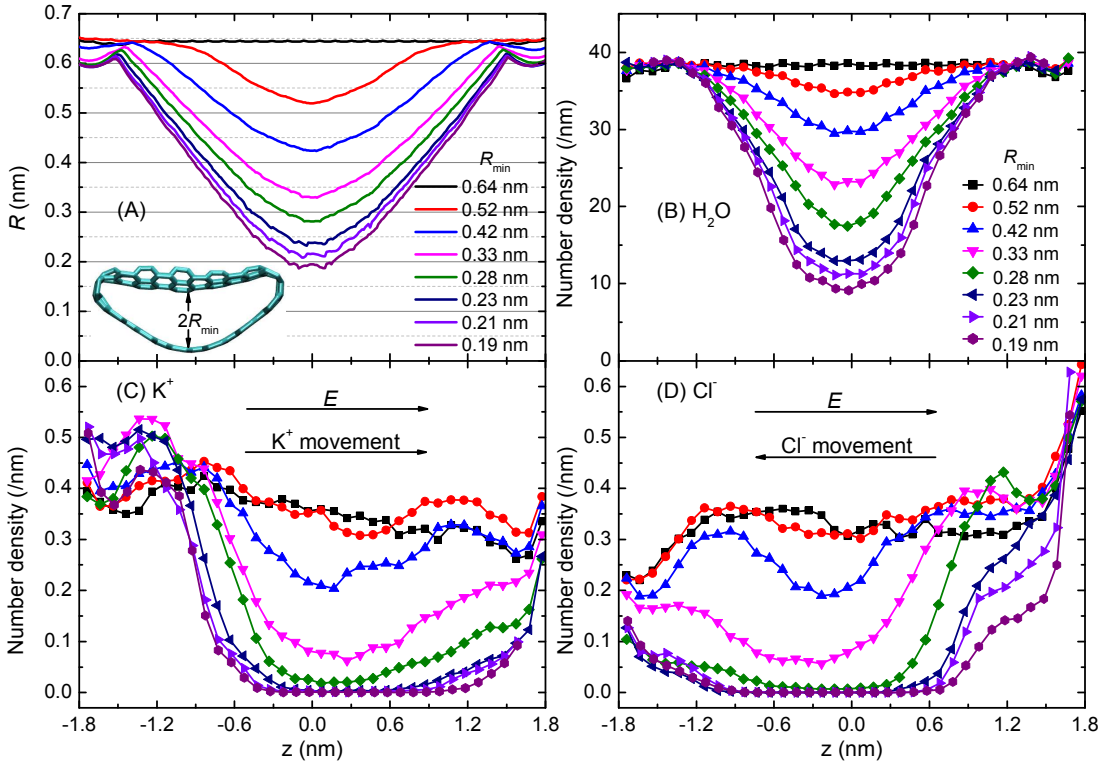


**Fig. 2** Radius ($R$) profiles (A) of CNT(12,12) with different deformation. Number density distributions of $H_2O$ (B), $K^+$ (C) and $Cl^-$ (D) in the direction defined by the tube axis (z axis) in CNT(12,12) with each deformation under the electric field $E$ = 0.1 V/nm. $R_{min}$ is the effective radius of the constriction formed in the tube midway (z = 0). The inset in panel (A) shows the cross-sectional view of the constriction and the definition of $R_{min}$. The directions of $E$ and the movements of $K^+$ and $Cl^-$ are shown in panels (C) and (D).

deformed tube may be suitable passing water while blocking ions as required in water desalination. When larger electric fields ($E$ = 0.15 and 0.2 V/nm) are applied, the ionic flux is still negligible for $R_{min}$ < 0.28 nm (Fig. S1B and S1C in the ESI†), indicating that the constriction with radius smaller than 0.28 nm is able to effectively close the channel to ionic conduction. It should be noted that the critical value of $R_{min}$ is smaller than that of some biological channels and model nanopores, as the large applied electric field in this work can help $K^+$ and $Cl^-$ to overcome the hindrance of the constriction to some extent. Moreover, the constriction gate is reversible. When the force on the tube with $R_{min}$ = 0.19 nm is removed, the local stress in the tube can make its shape recover to the undeformed one, and the ionic flux increases to the unperturbed level, as shown in Fig. 3. Additionally, the deformed tube exhibits a slight $K^+$ selectivity over $Cl^-$.

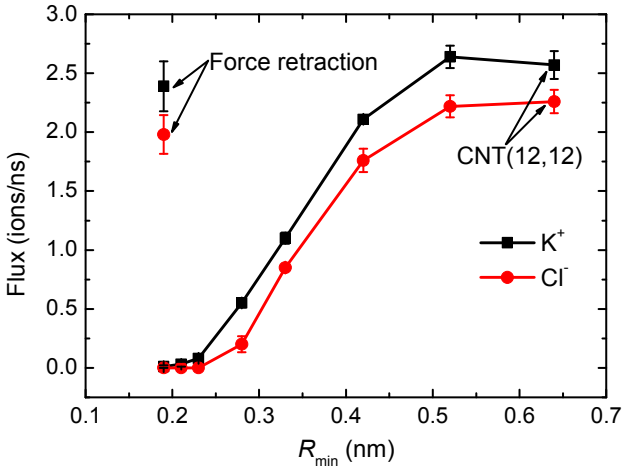


**Fig. 3** Ionic flux of $K^+$ and $Cl^-$ through CNT(12,12) with different deformation under $E$ = 0.1 V/nm. $R_{min}$ is the effective radius of the constriction. The flux on the force retraction and through the undeformed CNT(12,12) is labelled in the figure. Note that the $R_{min}$ value for the flux on the force retraction corresponds to the radius of the deformed tube from which the force was removed.

### The gating mechanism of the deformed channel

To figure out the gating mechanism of the deformed CNT(12,12), the potential of mean force (PMF), *i.e.*, the free energy profile of an ion passing through the tube was calculated and the ionic hydration states were analyzed. The results are plotted in Fig. 4. There is a energy barrier faced by $K^+$ (about 5.0 kJ/mol) and $Cl^-$ (about 8.0 kJ/mol) at the mouths of the tube (z = ±2.0 nm) for all the studied values of $R_{min}$. The energy barrier for $K^+$ entering the tube increases when the tube is gradually deformed, while the energy barrier for $Cl^-$ is almost not changed. This phenomenon may due to the weaker hydration of $K^+$ than that of $Cl^-$,[52,54,57] which makes its hydration at the tube mouths can be easily affected by other ions. The radii of the tube mouths (0.6-0.7 nm, shown in Fig. 2A) are larger than the radii of the first hydration shell of $K^+$ (0.36 nm) and $Cl^-$ (0.385 nm), and able to accommodate the entire inner hydration shells. Thus, this energy barrier is likely to be due to the rearrangement of the inner hydration shell and/or displacement of further hydration shells. In the bulk (z > 2.0 nm or z < -2.0 nm), the ion association and ion

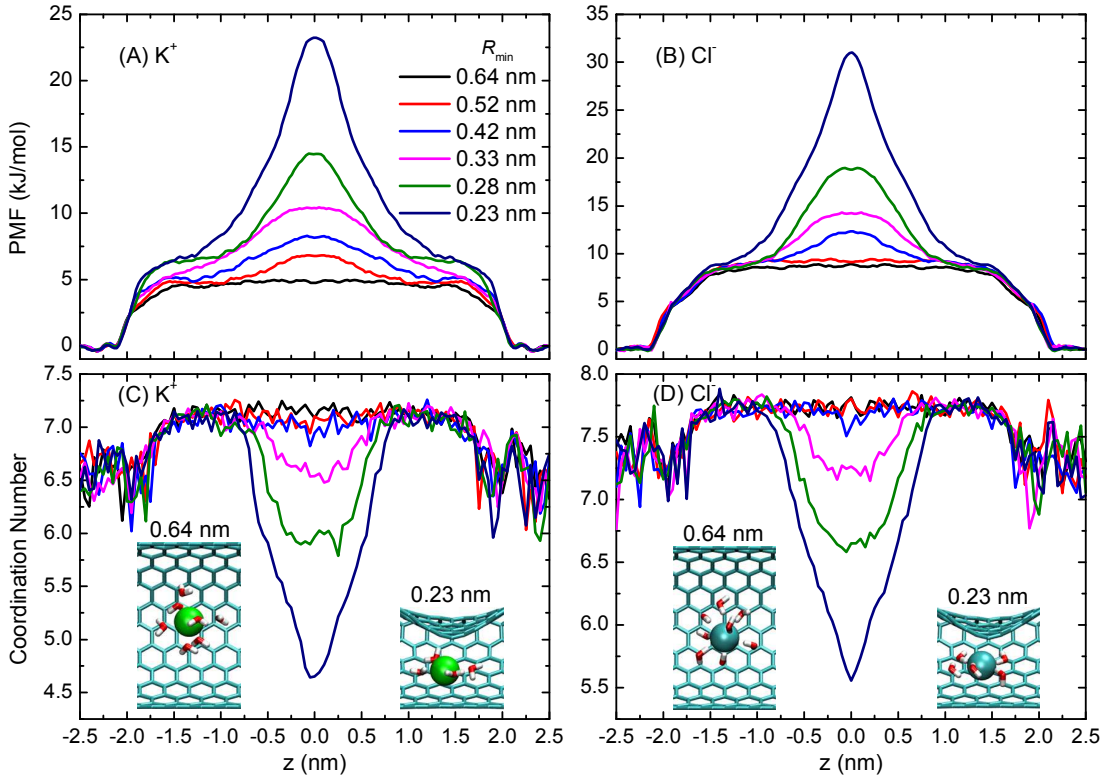


**Fig. 4** PMF and coordination number of $K^+$ (A, C) and $Cl^-$ (B, D) passing through CNT(12,12) with different deformation. $R_{min}$ is the effective radius of the constriction formed in the tube midway (z = 0). The insets show the typical configurations of the first hydration shells of $K^+$ and $Cl^-$ in the centre of the nanotube with $R_{min}$ = 0.64 and 0.23 nm.

pairing make the coordination numbers of $K^+$ and $Cl^-$ 0.5 smaller than those at the tube mouths.

For the undeformed CNT(12,12) with $R_{min}$ = 0.64 nm, no energy barrier is observed in the tube. When the tube is deformed, an additional energy barrier for $K^+$ and $Cl^-$ is established at the constriction (z = 0), as shown in Fig. 4A and 4B. For the constrictions with $R_{min}$ (0.52 and 0.42 nm) larger than the radii of first hydration shells of $K^+$ (0.36 nm) and $Cl^-$ (0.385 nm), $K^+$ and $Cl^-$ do not dehydrate at the constriction and their coordination numbers are similar to or slightly lower than those in the undeformed CNT(12,12), resulting in very small energy barriers. The transport through these two constrictions has small hindrance and relative large ionic flux is obtained, as shown in Fig. 3. Obvious ionic dehydration is observed when the constriction is smaller than the size of the first hydration shells, as shown in the insets of Fig. 4. For $R_{min}$ = 0.33, 0.28 and 0.23 nm, about 0.45, 1.18, 2.46 water molecules, and 0.58, 1.15, 2.24 water molecules are stripped from the first hydration shells of $K^+$ and $Cl^-$, respectively, as shown in Fig. 4C and 4D. The corresponding energy barriers at the constriction are much larger and increased dramatically with the decrease of $R_{min}$. Ion conduction through these narrower constrictions is highly hindered and results in a much smaller ionic flux, as displayed in Fig. 3. The energy barriers of $K^+$ and $Cl^-$ at the constrictions agree well with the previous explicitly calculated dehydration free energy,[57] which further confirms that the energy barriers are due to partial dehydration. For example, at the constriction with $R_{min}$ = 0.28 nm, the coordination number of $K^+$ drops to 5.9 and the energy barrier is about 15.0 kJ/mol, close to the dehydration energy of 16.7 kJ/mol of $K^+$ surrounded by 6 water molecules.[57] In addition, the energy barrier of $Cl^-$ is always higher than that of $K^+$ for the same constrictions, which accounts for the larger flux of $K^+$ (Fig. 3).

The large energy barriers at the constriction indicate that it is impossible for several ions staying at the constriction simultaneously, which is evidenced by an extremely low ionic density at the constriction (Figs. 2C and 2D). Moreover, under electric fields, the conduction of $K^+$ and $Cl^-$ through the constriction is in single-ion form, and ion-ion interaction can be only observed near the tube mouths. Therefore, the effect of concentration on ion conduction through the constriction and its critical block radius can be neglected.

The applied force on CNT(12,12) generates a constriction in the tube and induces partial dehydration of $K^+$ and $Cl^-$ at the hydrophobic constriction, as a result, the insurmountable energy barrier blocks the ion conduction and closes the tube. This mechanical gating mechanism of the deformed hydrophobic tube is quite similar to the hydrophobic gating in biological channels.[34,35] For example, at the hydrophobic constriction of the MscS channel, about one-half of the water molecules in the first hydration shell of $Cl^-$ were depleted and resulted in a 41.8 kJ/mol barrier.[40] The 0.3 nm radius non-polar gate in nAChR hinders ion conduction by presenting 26.2 and 16.2 kJ/mol barriers to $Na^+$ and $Cl^-$, respectively.[35] Nevertheless, we found that the full dewetting of hydrophobic gates in biological channels may be not necessarily required to close the channels, as partial dehydration of ions in the continuous water-filled constrictions of CNT(12,12) in this work is enough to block ion conduction.

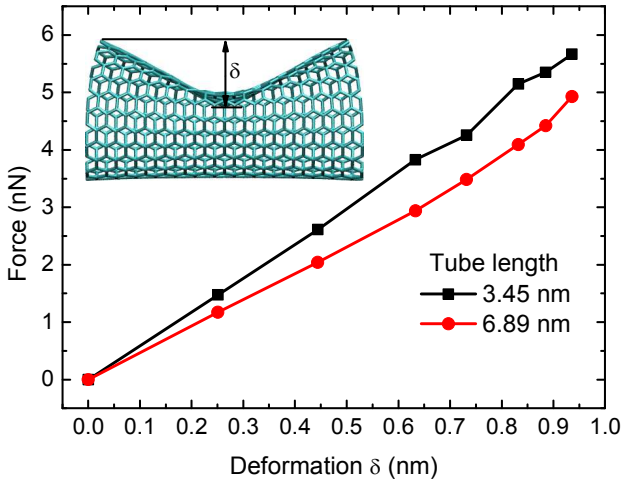


**Fig. 5** The relationship between the exerted force and the tube deformation δ of CNT(12,12) with length of 3.45 nm and 6.89 nm. The inset illustrates the definition of tube deformation δ.

**Feasibility of the mechanical nanogate**

To test whether the deformation of CNT(12,12) in this work is feasible in experiments, constant velocity and constant force SMD simulations, which emulate the process of an atomic force microscope (AFM) tip acting on the tube, were performed to determine the magnitude of the force exerted on the tube to form a constriction with effective radius $R_{min}$. The simulation results are shown in Fig. 5. During the SMD simulations, the centre of the tube was laterally deformed continuously until the elastic force of the tube increased to the exerted force, *i.e.*, an equilibrium state corresponding to a constriction with $R_{min}$ was reached. The force required to deform CNT(12,12) is on the order of nN, which is comparable to the previous experimental and theoretic values.[73,74] The mechanical deformation of the tube may conform to the Hooke's law, as a good linear relationship between the force and the deformation was observed, as shown in Fig. 5. Given that the length of CNT used in nanofluidic systems[73,75] is much longer than the tube used here, we explore the effect of the tube length on the force required to deform it by considering a tube with twice length 6.89 nm. It is found that the force tends to decrease with the tube length. It is found that to achieve the same deformation δ, smaller force is required for the CNT with a length of 6.89 nm than the CNT of 3.45 nm in length, indicating that smaller force may be required for longer CNTs.

To summarize our results, the coordination numbers, energy barriers and flux of $K^+$ and $Cl^-$ through the nanotube is plotted against the exerted force in Fig. 6. When the applied force is smaller than 4 nN ($R_{min}$ > 0.28 nm), $K^+$ and $Cl^-$ are only slightly dehydrated and encounter only small energy barriers and so their fluxes are considerable. For force larger than 5 nN, partial dehydration is observed and the resultant large energy barrier makes the flux negligible, as shown in Fig. 6C. The force of 5.67 nN is able to completely close the tube for ion conduction. The magnitude of the force required to gate the tube falls in the working range of many available experimental facilities.[76] Moreover, it has been experimentally demonstrated that a CNT can be deformed by an AFM tip[73] and this mechanical deformation was found to be reversible.[77,78] In the SMD simulations, we find that the tube can be deformed only with

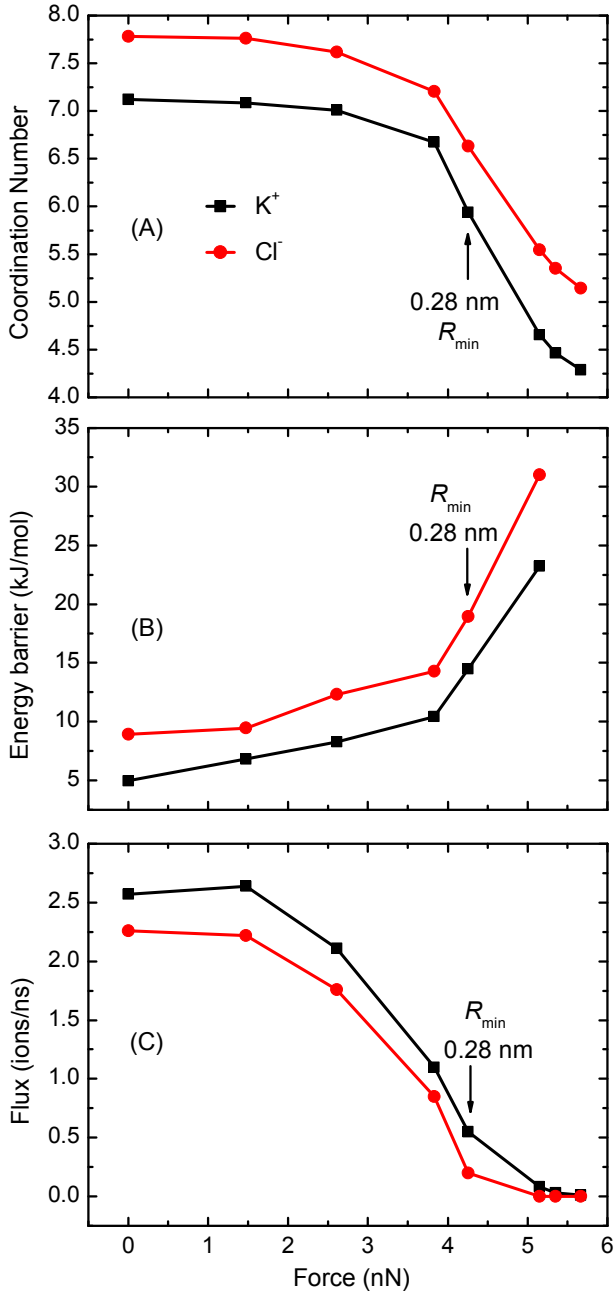


**Fig. 6** The coordination numbers (A), energy barriers (B) of $K^+$ and $Cl^-$ at the constriction of the tube, and their flux through CNT(12,12) under each magnitude of exerted force.

large spring constant. Thus, atomically sharp and stiff AFM tips should be used, given the small size of the tube. However, the smallest AFM tip has a radius below 10 nm. We speculate that the longer tube may be deformed by a larger AFM tip and its gating function takes effect, though the shape of the deformed tube in this work can not be exactly reproduced. In addition, the previously reported methods of fabricating CNT-based nanofludic devices with the use of an epoxy structure[16,75] can be followed to build the system designed here. Therefore, the design of the mechanical nanovalve based on CNT(12,12) in this work for gating ion conduction may be feasible.

The nanogate designed here can be generalized to control a wide range of substances. It is applicable to divalent ions, such as $Ca^{2+}$ and $Mg^{2+}$, as their dehydration energies are higher than that of monovalent ions due to much stronger electrostatic interactions between them and water molecules.[79] CNTs with proper diameter should be chosen according to the size of the studied ions, e.g. larger CNTs for $NO_3^-$, $SO_4^{2-}$ and $NH_4^+$. Apart from deforming a CNT, there are other methods to control ion conduction. It is possible to selectively transport ions by modulating the surface charge of the CNT.[18] Positing an external charge and changing its distance to the CNT[6] to control the electrostatic interactions may be another approach to manipulate the transport of charged species in the CNT. In addition, the steric occlusion effect of the deformed CNT can be also used to control the transport of molecules, such as water molecules. This mechanical deformed CNT by AFM tips have many potential applications, such as a nanovalve in nanofluidic systems to reversibly control the ionic flows and a high-performance nanodevice for desalination and water treatment.

## Conclusions

In summary, inspired by the hydrophobic gating mechanism in biological ion channels, we performed molecular dynamics simulations to design a CNT(12,12) based nanogate. The simulation results show that, under the influence of an external force, the CNT(12,12) is deformed and a hydrophobic constriction is formed in the tube centre, which can act as a gate to control ion conduction. With the external force increasing, the effective radius $R_{min}$ of the constriction is gradually reduced and ions face increasing barriers to pass through the pore. For $R_{min}$ < 0.33 nm, the constriction is almost vacant of ions and obviously hinders the ion conduction, resulting in enrichments of $K^+$ and $Cl^-$ on the left and right sides of the constriction, respectively. When the exerted external force is larger than 5 nN, the constriction with a radius smaller than 0.23 nm is able to close the tube for ion conduction, while allowing water molecules to pass through. This nanogate is reversible, as the ionic fluxes can revert back to the unperturbed level upon the force retraction. It is found that, in the hydrophobic constriction of the tube, stripping 40 % and 34 % of the water molecules in the first hydration shells of $K^+$ and $Cl^-$ can effectively and completely block ion conduction under 0.1 V/nm, even though the constriction has an effective radius of 0.19 nm and is water filled. Thus, the full dewetting of the gate is not required to close the channel as suggested for biological pores. The force required to deform the tube increases linearly with the deformation and may be exerted by atomically sharp and stiff AFM tips. This biomimetic and mechanical nanogate based on CNT(12,12) can serve as a reversible device to control mass transport in nanofluidic devices.

## Acknowledgements

This work was supported by the National Key Basic Research Program of China (No.2013CB733500), National Natural Science Foundation of China (Nos.21376089, 91334202) and the Fundamental Research Funds for the Central Universities (SCUT-2013ZM0073). The computational resources for this project are provided by SCUTGrid at South China University of Technology and the National Supercomputing Centre in Shenzhen (China). and additional computer time from the National Computational Infrastructure (NCI) National Facility (Australia). Z.H. thanks the China Scholarship Council for support.

## Notes and references

[a] *School of Chemistry and Chemical Engineering, South China University of Technology, Guangzhou, Guangdong 510640, China. Tel: +86 02 87114069; E-mail: jianzhou@scut.edu.cn*
[b] *Research School of Biology, The Australian National University, Canberra ACT 0200, Australia.*
[c] *State Key Laboratory of Materials-oriented Chemical Engineering, Nanjing University of Technology, Nanjing 210009, China*

† Electronic Supplementary Information (ESI) available: Water flux under 0.1V/nm and ionic flux under 0.15 and 0.2 V/nm. See DOI: 10.1039/b000000x/

1. B. Hille, *Ionic Channels of Excitable Membranes*, Sinauer Associates Inc.: Sunderland, MA, 2001.
2. M. Majumder, N. Chopra, R. Andrews and B. J. Hinds, *Nature*, 2005, **438**, 44.
3. J. K. Holt, H. G. Park, Y. M. Wang, M. Stadermann, A. B. Artyukhin, C. P. Grigoropoulos, A. Noy and O. Bakajin, *Science*, 2006, **312**, 1034-1037.
4. A. Kalra, S. Garde and G. Hummer, *Proc. Natl. Acad. Sci. U. S. A.*, 2003, **100**, 10175-10180.
5. R. Z. Wan, J. Y. Li, H. J. Lu and H. P. Fang, *J. Am. Chem. Soc.*, 2005, **127**, 7166-7170.
6. J. Y. Li, X. J. Gong, H. J. Lu, D. Li, H. P. Fang and R. H. Zhou, *Proc. Natl. Acad. Sci. U. S. A.*, 2007, **104**, 3687-3692.
7. X. J. Gong, J. Y. Li, H. Zhang, R. Z. Wan, H. J. Lu, S. Wang and H. P. Fang, *Phys. Rev. Lett.*, 2008, **101**, 257801.
8. O. Beckstein and M. S. P. Sansom, *Proc. Natl. Acad. Sci. U. S. A.*, 2003, **100**, 7063-7068.
9. R. Qiao and N. R. Aluru, *Phys. Rev. Lett.*, 2004, **92**, 198301.
10. R. Qiao, J. G. Georgiadis and N. R. Aluru, *Nano Lett.*, 2006, **6**, 995-999.
11. C. Peter and G. Hummer, *Biophys. J*. 2005, **89**, 2222-2234.
12. H. M. Liu, S. Murad and C. J. Jameson, *J. Chem. Phys.*, 2006, **125**, 084713.
13. T. A. Beu, *J. Chem. Phys.*, 2011, **135**, 044516.
14. Z. J. He and J. Zhou, *Acta Chim. Sinica*, 2011, **69**, 2901-2907.
15. C. Ho, R. Qiao, J. B. Heng, A. Chatterjee, R. J. Timp, N. R. Aluru and G. Timp, *Proc. Natl. Acad. Sci. U. S. A.*, 2005, **102**, 10445-10450.
16. J. Wu, K. Gerstandt, H. B. Zhang, J. Liu and B. J. Hinds, *Nat. Nanotechnol.*, 2012, **7**, 133-139.
17. A. Rios, M. Zougagh and M. Avila, *Anal. Chim. Acta*, 2012, **740**, 1-11.
18. J. H. Park, S. B. Sinnott and N. R. Aluru, *Nanotechnology*, 2006, **17**, 895-900.
19. H. Y. Chen, X. G. Gong, Z. F. Liu and D. Y. Sun, *J. Phys. Chem. C*, 2011, **115**, 4721-4725.
20. Y. S. Tu, R. H. Zhou and H. P. Fang, *Nanoscale*, 2010, **2**, 1976-1983.
21. K. K. Coti, M. E. Belowich, M. Liong, M. W. Ambrogio, Y. A. Lau, H. A. Khatib, J. I. Zink, N. M. Khashab and J. F. Stoddart, *Nanoscale*, 2009, **1**, 16-39.

22. S. P. Adiga and D. W. Brenner, *Nano Lett.*, 2005, **5**, 2509-2514.
23. A. Kocer, M. Walko, W. Meijberg and B. L. Feringa, *Science*, 2005, **309**, 755-758.
24. L. M. Yang, R. Wray, J. Parker, D. Wilson, R. S. Duran and P. Blount, *ACS Nano*, 2012, **6**, 1134-1141.
25. S. R. Wang, Z. Y. Liang, B. Wang, C. Zhang and Z. Rahman, *Nanotechnology*, 2007, **18**, 055301.
26. H. J. Dai, *Acc. Chem. Res.*, 2002, **35**, 1035-1044.
27. M. Majumder, X. Zhan, R. Andrews and B. J. Hinds, *Langmuir*, 2007, **23**, 8624-8631.
28. M. A. Yu, H. H. Funke, J. L. Falconer and R. D. Noble, *J. Am. Chem. Soc.*, 2010, **132**, 8285-8290.
29. X. J. Gong, J. C. Li, C. Guo, K. Xu and H. Yang, *Nanotechnology*, 2013, **24**, 025502.
30. A. Miyazawa, Y. Fujiyoshi and N. Unwin, *Nature*, 2003, **423**, 949-955.
31. D. A. Doyle, J. M. Cabral, R. A. Pfuetzner, A. L. Kuo, J. M. Gulbis, S. L. Cohen, B. T. Chait and R. MacKinnon, *Science*, 1998, **280**, 69-77.
32. R. J. C. Hilf and R. Dutzler, *Nature*, 2008, **452**, 375-379.
33. R. B. Bass, P. Strop, M. Barclay and D. C. Rees, *Science*, 2002, **298**, 1582-1587.
34. B. Corry, *Biophys. J* . 2006, **90**, 799-810.
35. O. Beckstein and M. S. P. Sansom, *Phys. Biol.*, 2006, **3**, 147-159.
36. M. O. Jensen, D. W. Borhani, K. Lindorff-Larsen, P. Maragakis, V. Jogini, M. P. Eastwood, R. O. Dror and D. E. Shaw, *Proc. Natl. Acad. Sci. U. S. A.*, 2010, **107**, 5833-5838.
37. H. Nury, F. Poitevin, C. Van Renterghem, J. P. Changeux, P. J. Corringer, M. Delarue and M. Baaden, *Proc. Natl. Acad. Sci. U. S. A.*, 2010, **107**, 6275-6280.
38. F. Q. Zhu and G. Hummer, *Proc. Natl. Acad. Sci. U. S. A.*, 2010, **107**, 19814-19819.
39. C. Song and B. Corry, *Biophys. J* . 2010, **98**, 404-411.
40. A. Anishkin and S. Sukharev, *Biophys. J* . 2004, **86**, 2883-2895.
41. V. Vasquez, M. Sotomayor, J. Cordero-Morales, K. Schulten and E. Perozo, *Science*, 2008, **321**, 1210-1214.
42. J. P. Birkner, B. Poolman and A. Kocer, *Proc. Natl. Acad. Sci. U. S. A.*, 2012, **109**, 12944-12949.
43. O. Beckstein, P. C. Biggin and M. S. P. Sansom, *J. Phys. Chem. B*, 2001, **105**, 12902-12905.
44. O. Beckstein and M. S. P. Sansom, *Phys. Biol.*, 2004, **1**, 42-52.
45. B. Corry, *J. Phys. Chem. B*, 2008, **112**, 1427-1434.
46. Q. Shao, J. Zhou, L. H. Lu, X. H. Lu, Y. D. Zhu and S. Y. Jiang, *Nano Lett.*, 2009, **9**, 989-994.
47. L. A. Richards, A. I. Schafer, B. S. Richards and B. Corry, *Small*, 2012, **8**, 1701-1709.
48. L. A. Richards, A. I. Schafer, B. S. Richards and B. Corry, *Phys. Chem. Chem. Phys.*, 2012, **14**, 11633-11638.
49. L. A. Richards, B. S. Richards, B. Corry and A. I. Schäfer, *Environ. Sci. Technol.*, 2013, **47**, 1968-1976.
50. Z. J. He, J. Zhou, X. H. Lu and B. Corry, *J. Phys. Chem. C*, 2013, **117**, 11412-11420.
51. Z. J. He, J. Zhou, X. H. Lu and B. Corry, *ACS Nano*, 2013, 10148-10157.
52. J. Zhou, X. H. Lu, Y. R. Wang and J. Shi, *Fluid Phase Equilib.*, 2002, **194**, 257-270.
53. H. J. Feng, J. Zhou, X. H. Lu and K. A. Fichthorn, *J. Chem. Phys.*, 2010, **133**, 061103.
54. Q. Shao, L. L. Huang, J. Zhou, L. H. Lu, L. Z. Zhang, X. H. Lu, S. Y. Jiang, K. E. Gubbins and W. F. Shen, *Phys. Chem. Chem. Phys.*, 2008, **10**, 1896-1906.
55. Y. D. Zhu, J. Zhou, X. H. Lu, X. J. Guo and L. H. Lu, *Microfluid. Nanofluid.*, 2013, **15**, 191-205.
56. H. M. Liu, C. J. Jameson and S. Murad, *Mol. Simul.*, 2008, **34**, 169-175.
57. C. Song and B. Corry, *J. Phys. Chem. B*, 2009, **113**, 7642-7649.
58. Y. X. Jiang, A. Lee, J. Y. Chen, M. Cadene, B. T. Chait and R. MacKinnon, *Nature*, 2002, **417**, 523-526.
59. N. Unwin, *Nature*, 1995, **373**, 37-43.
60. A. D. J. MacKerell, D. Bashford, Bellott, R. L. Dunbrack, J. D. Evanseck, M. J. Field, S. Fischer, J. Gao, H. Guo, S. Ha, D. Joseph-McCarthy, L. Kuchnir, K. Kuczera, F. T. K. Lau, C. Mattos, S. Michnick, T. Ngo, D. T. Nguyen, B. Prodhom, W. E. Reiher, B. Roux, M. Schlenkrich, J. C. Smith, R. Stote, J. Straub, M. Watanabe, J. Wiórkiewicz-Kuczera, D. Yin and M. Karplus, *J. Phys. Chem. B*, 1998, **102**, 3586-3616.
61. W. L. Jorgensen, J. Chandrasekhar, J. D. Madura, R. W. Impey and M. L. Klein, *J. Chem. Phys.*, 1983, **79**, 926-935.
62. A. Mehta, E. J. Nelson, S. M. Webb and J. K. Holt, *Adv. Mater.*, 2009, **21**, 102-106.
63. P. A. Cazade, J. Dweik, B. Coasne, F. Henn and J. Palmeri, *J. Phys. Chem. C*, 2010, **114**, 12245-12257.
64. T. A. Beu, *J. Chem. Phys.*, 2010, **132**, 164513.
65. T. Darden, D. York and L. Pedersen, *J. Chem. Phys.*, 1993, **98**, 10089-10092.
66. S. Nose, *Mol. Phys.*, 1984, **52**, 255-268.
67. M. Parrinello and A. Rahman, *J. Appl. Phys.*, 1981, **52**, 7182-7190.
68. B. Hess, C. Kutzner, D. van der Spoel and E. Lindahl, *J. Chem. Theory Comput.*, 2008, **4**, 435-447.
69. G. M. Torrie and J. P. Valleau, *Chem. Phys. Lett.*, 1974, **28**, 578-581.
70. S. Kumar, D. Bouzida, R. H. Swendsen, P. A. Kollman and J. M. Rosenberg, *J. Comput. Chem.*, 1992, **13**, 1011-1021.
71. H. Grubmuller, B. Heymann and P. Tavan, *Science*, 1996, **271**, 997-999.
72. O. S. Smart, J. G. Neduvelil, X. Wang, B. A. Wallace and M. S. P. Sansom, *J. Mol. Graphics*, 1996, **14**, 354-360.
73. T. W. Tombler, C. W. Zhou, L. Alexseyev, J. Kong, H. J. Dai, L. Lei, C. S. Jayanthi, M. J. Tang and S. Y. Wu, *Nature*, 2000, **405**, 769-772.
74. Y. R. Jeng, P. C. Tsai and T. H. Fang, *J. Chem. Phys.*, 2005, **122**, 224713.
75. C. Y. Lee, W. Choi, J. H. Han and M. S. Strano, *Science*, 2010, **329**, 1320-1324.
76. E. Meyer, *Prog. Surf. Sci.*, 1992, **41**, 3-49.
77. L. Liu, C. S. Jayanthi, M. J. Tang, S. Y. Wu, T. W. Tombler, C. W. Zhou, L. Alexseyev, J. Kong and H. J. Dai, *Phys. Rev. Lett.*, 2000, **84**, 4950-4953.
78. A. Maiti, *Chem. Phys. Lett.*, 2000, **331**, 21-25.
79. B. Corry, *PeerJ*, 2013, **1**, e16, DOI: 10.7717/peerj.16.